AGU PUBLICATIONS

Geophysical Research Letters

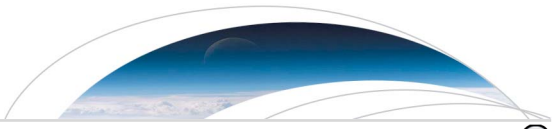

RESEARCH LETTER
10.1002/2017GL075583

Key Points:
- Three climate models driven by observed sea surface temperatures increase then decrease climate sensitivity over the twentieth century
- Substantial changes of the climate feedback parameter are mirrored by the global mean low-level cloud anomalies
- This variability is connected to atmospheric stability and not dominated by stratocumulus regions, but by the broader tropics

Supporting Information:
- Supporting Information S1

Correspondence to:
L. G. Silvers,
silvers@princeton.edu

Citation:
Silvers, L. G., Paynter, D., & Zhao, M. (2018). The diversity of cloud responses to twentieth century sea surface temperatures. *Geophysical Research Letters*, *45*, 391–400. https://doi.org/10.1002/2017GL075583

Received 7 SEP 2017
Accepted 5 DEC 2017
Accepted article online 11 DEC 2017
Published online 4 JAN 2018

©2017. The Authors.
This is an open access article under the terms of the Creative Commons Attribution-NonCommercial-NoDerivs License, which permits use and distribution in any medium, provided the original work is properly cited, the use is non-commercial and no modifications or adaptations are made.

The Diversity of Cloud Responses to Twentieth Century Sea Surface Temperatures

Levi G. Silvers[1], **David Paynter**[2], **and Ming Zhao**[2]

[1]GFDL, Princeton University, Princeton, NJ, USA, [2]GFDL/NOAA, Princeton, NJ, USA

Abstract Low-level clouds are shown to be the conduit between the observed sea surface temperatures (SST) and large decadal fluctuations of the top of the atmosphere radiative imbalance. The influence of low-level clouds on the climate feedback is shown for global mean time series as well as particular geographic regions. The changes of clouds are found to be important for a midcentury period of high sensitivity and a late century period of low sensitivity. These conclusions are drawn from analysis of amip-piForcing simulations using three atmospheric general circulation models (AM2.1, AM3, and AM4.0). All three models confirm the importance of the relationship between the global climate sensitivity and the eastern Pacific trends of SST and low-level clouds. However, this work argues that the variability of the climate feedback parameter is not driven by stratocumulus-dominated regions in the eastern ocean basins, but rather by the cloudy response in the rest of the tropics.

1. Introduction

Determining how the atmosphere responds to anthropogenic forcing is complicated by the strong decadal variability which is present in the global mean top of the atmosphere (TOA) flux of energy (N, W m^{-2}). Over the historical period (post-1870) these fluctuations of N include forced (natural and anthropogenic) and internal variability. One measure of the climate sensitivity is to regress N under fixed radiative forcing versus the change of surface air temperature T as the atmosphere adjusts to a radiative perturbation (Gregory et al., 2004). The climate feedback parameter α (W m^{-2} K^{-1}) is then given by the slope of the regression line. This technique has been applied to climate models forced with historical SSTs and fixed radiative forcing to obtain an estimate of α over the historical period. Previously examined models (Gregory and Andrews, 2016; Zhou et al., 2016, GA16 and Z16 hereafter, respectively) have shown a period of high sensitivity (small α over 1925–1955), followed by a period of low sensitivity (large α over 1975–2005), irrespective of their long-term or equilibrated sensitivity. It has been conjectured (Z16) that an increase of eastern Pacific low-level clouds played a significant role in the low sensitivity of the later period. To our knowledge, the influence of clouds on the global energy budget during the high sensitivity early period has not been investigated. This raises several questions. What role do clouds over the rest of the globe play? Can the decadal variability of α be explained by low-cloud, or stratocumulus-dominated regions like the Eastern Pacific? If so, what do these cloud-based influences on the Earth's energy budget tell us about the cloud feedback that we should expect in future climates?

The impact of low-cloud cover on the radiation budget of Earth has been the source of active research for decades (e.g., Bony et al., 2004; Bony & Dufresne, 2005; Klein & Hartmann, 1993; Randall et al., 1984). Recently, Qu et al. (2014, 2015) provided a thorough examination of the dependencies between low-cloud cover, the estimated inversion strength (EIS), and surface temperature in both observations, and an ensemble of models from CMIP3 and CMIP5. They, as did most previous studies (e.g., Klein & Hartmann, 1993; Wood & Bretherton, 2006), focused on five oceanic regions which are important for stratocumulus decks of radiatively active low-level clouds. Only recently have the fields of stability, low-level clouds, and low-level temperature begun to be investigated over larger swaths of the globe (Grise & Medeiros, 2016; Rose & Rayborn, 2016; Webb et al., 2015; Zhou et al., 2016).

A linearized forcing-feedback framework has often been used to study the global mean energy budget and assess α despite its known temporal variations (e.g., Andrews et al., 2015; Armour, 2017; Armour et al., 2013; Forster & Gregory, 2006; GA16; Gregory et al., 2004; Mauritsen et al., 2013; Proistosescu & Huybers, 2017; Rose et al., 2014; Senior & Mitchell, 2000; Winton et al., 2010). Decadal variability of the energy budget has been

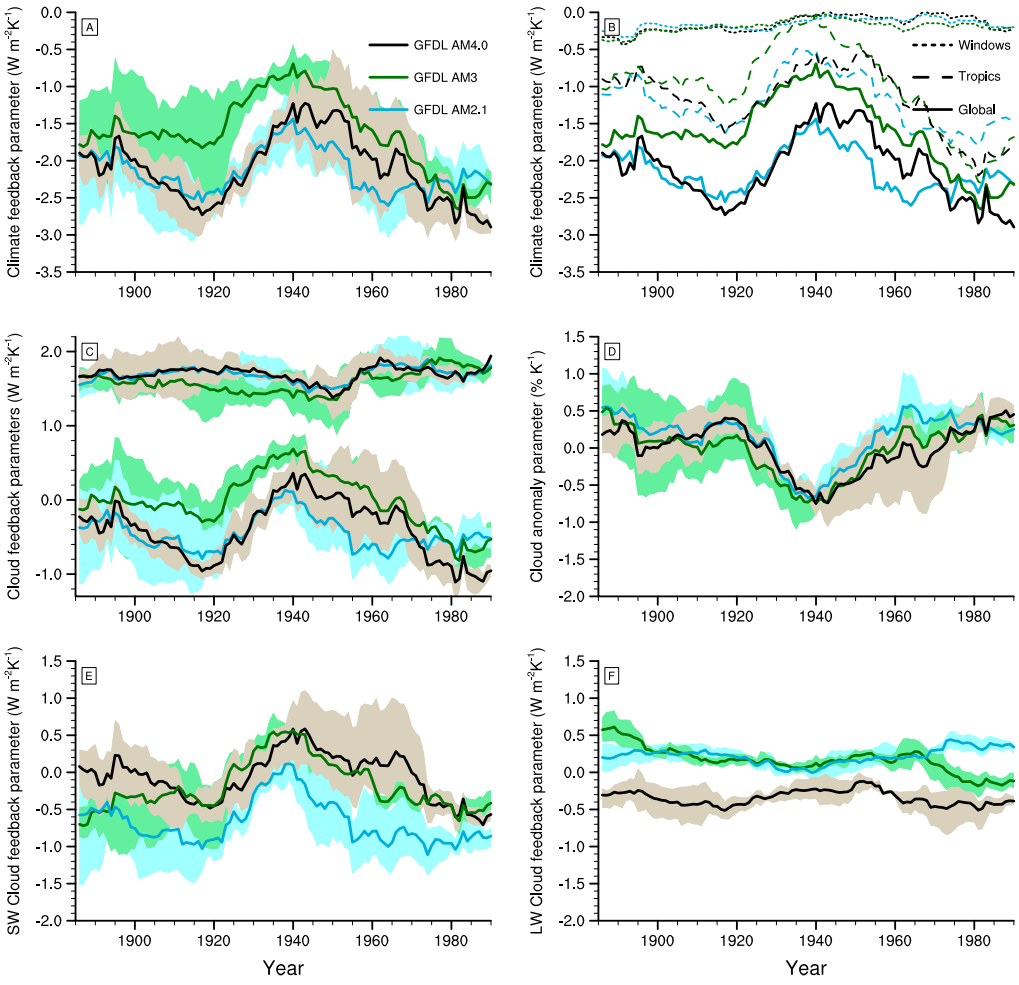

Figure 1. Time series analysis of AM4.0 (black), AM3 (green), and AM2.1 (blue). Thick lines are ensemble means; shading gives range of ensemble members. (a) Global climate feedback parameter $-\alpha$ (W/m^2 K). (b) Same as Figure 1a but with contributions from four tropical windows (short dash) and the rest of tropics (long dash). (c) α (W/m^2 K) decomposed into the CRE (lower) and CLR (upper) components. (d) Global mean low-cloud cover parameter LCC_{LR} (%/K). Global α_{CRE} (W/m^2 K) is decomposed into the (e) short-wave CRE and the (f) long-wave CRE. All time series computed by regression against global, yearly mean surface air temperature change.

shown to be particularly pronounced in both α, and the cloud radiative effect (CRE; Figures 1a, 1c, 1e, and 1f, GA16; Z16). A better understanding of the role played by clouds in determining α will be useful regardless of whether the changes are due to radiative forcings, natural variability, anthropogenic influences, or changes in the uptake of heat into the oceans (Haugstad et al., 2017).

This paper examines the atmospheric response to prescribed SST patterns in simulations of the years 1870–2005. The use of three atmospheric general circulation models (AGCMs) developed at the Geophysical Fluid Dynamics Laboratory (GFDL; AM2.1, AM3, and AM4.0) provides a comparison of models with significantly different treatments of the clouds. Interdecadal variability of the global feedback parameter has been previously studied (GA16; Z16) but the regional differences between cloud fields during periods of differing sensitivity are still not clearly understood. These experiments preclude an analysis of atmosphere-ocean feedback processes, or a direct prediction of how the climate would respond to forcing perturbations. However, we utilize the best estimate of observed SST and sea ice concentrations to facilitate an analysis of how AGCMs respond to these boundary conditions. By identifying the response of AGCMs to key geographic regions of change, we intend to move closer to a process level understanding of the connection between SST patterns, clouds, and the climate sensitivity.

2. Methods

2.1. Description of Amip-PiForcing Experiments, AM2.1, AM3, and AM4.0

This work uses the amip-piForcing experiment to investigate the atmospheric response to surface forcing between the years 1870 and 2005. The experiment drives AGCMs with observationally based SST and sea ice concentrations, while the forcing due to greenhouse gases, aerosol, and solar forcing is held constant at assumed preindustrial levels. However, due to the different time at which these models were actively used, the SST and sea ice fields differed slightly among models. The amip-piForcing experiment develops some of the ideas from Andrews (2014) and is one of the CFMIP3 experiments; for additional details and examples see Webb et al. (2017), GA16, and Z16. For each of the three AGCMs, five ensemble members have been used. Three distinct models are used to demonstrate the robustness of the cloud feedback response.

Cumulus cloud parameterizations are one of the largest differences among the GFDL atmospheric models analyzed here. The AM2.1 model uses the Relaxed-Arakawa-Schubert (Moorthi & Suarez, 1992) scheme; AM3 uses the Donner-Deep scheme for deep convection (Donner, 1993) and the University of Washington scheme (UWShCu, Bretherton et al., 2004) for shallow convection. AM4.0 uses a version of the UWShCu scheme that has been modified to include two bulk plumes which account for shallow and deep convection. Documentation of the GFDL AGCMS can be found in GFDL-GAMDT (2004), Donner et al. (2011), and AM4.0 will be documented with manuscripts which are currently in preparation. Some of the details of the convection scheme in AM4.0 are given in Zhao et al. (2016), and a study looking at the influence of CREs on the intertropical convergence zone with a recent prototype AM4 in aquaplanet mode are described in Popp and Silvers (2017).

2.2. Methodology of Analysis

We are interested in the influence of clouds on the decadal variability of the TOA net global mean radiative flux (N). As in GA16 the global mean energy budget is given by $N = F - \alpha T$, where we have assumed that $R = \alpha T$ and α is the climate feedback parameter. Our interest is in the covariation of R (global mean TOA radiative flux change due to some perturbation to the climate) and T (global mean surface air temperature change) rather than the change relative to a control state. Smaller values of α require a larger T to balance the imposed perturbation to the system. We compute the climate feedback parameter in the same way as in GA16 (their differential climate feedback parameter $\tilde{\alpha}$). That is, linear regression is used to compute the relationship between R and T, given by α. The regression is applied to the global yearly mean values over moving 30 year windows. In the same way we have computed the covariation of the CRE, short-wave (SW) CRE, long-wave (LW) CRE, and the clear-sky fluxes with T, as well as the anomalous global low-cloud cover (LCC; clouds below 680 hPa) with T (α_{CRE}, $\alpha_{\mathrm{SW\,CRE}}$, $\alpha_{\mathrm{LW\,CRE}}$, α_{CLR}, and $\mathrm{LCC}_{\mathrm{LR}}$, respectively; LR denoting linear regression method). These time series are shown in Figure 1 with each point representing the midpoint of a 30 year window. We emphasize that the terminology "climate sensitivity" and "climate feedback parameter" here simply refer to measures of the change of radiative balance at TOA with fixed radiative forcing and prescribed SST. This method of computing climate sensitivity is in keeping with previous studies (Cess et al., 1989; Silvers et al., 2016; GA16), and we assume there is useful correspondence between the interaction of clouds and the TOA energy budget found here and in a fully coupled Earth system. For amip-piForcing experiments, $F = 0$, and the "effective" climate sensitivity can be inferred as $F_{2\times}/\alpha$, where $F_{2\times}$ is an appropriate representative value of radiative forcing due to doubled (relative to preindustrial) CO_2 concentrations (we use $F_{2\times} = 3.4\,\mathrm{W\,m^{-2}}$, Flato et al., 2013). This is distinct from the equilibrium climate sensitivity (ECS), defined as the equilibrium response to doubled CO_2 concentrations.

The strong connection between global clouds and α is shown in Figure 1. To investigate the spatial patterns of this connection, we use linear regression to compute trends over time at each grid point for SST, SW CRE, LW CRE, LCC, and EIS (Figures 2 and 3a). Global figures focus on ocean regions because it is primarily there that low stratiform clouds are found.

Previous studies have shown lower tropospheric stability (LTS) to be a useful diagnostic tool that connects low-cloud changes to the characteristics of the large-scale environment, especially within traditionally defined stratocumulus regions (Klein & Hartmann, 1993; Medeiros et al., 2008; Webb et al., 2015; Wood & Bretherton, 2006). We analyze the EIS, which can be thought of as a correction to the LTS based on the moist adiabatic profile. The LTS used by Klein and Hartmann (1993) was defined as $\mathrm{LTS} = \theta_{700\,\mathrm{hPa}} - \theta_{\mathrm{sfc}}$, where θ is the potential temperature and the subscript indicates the level at which the values are taken. For EIS we use the approximation made by Wood and Bretherton (2006):

$$\mathrm{EIS} = \mathrm{LTS} - \Gamma_m^{850}(z_{700} - \mathrm{LCL}) \tag{1}$$

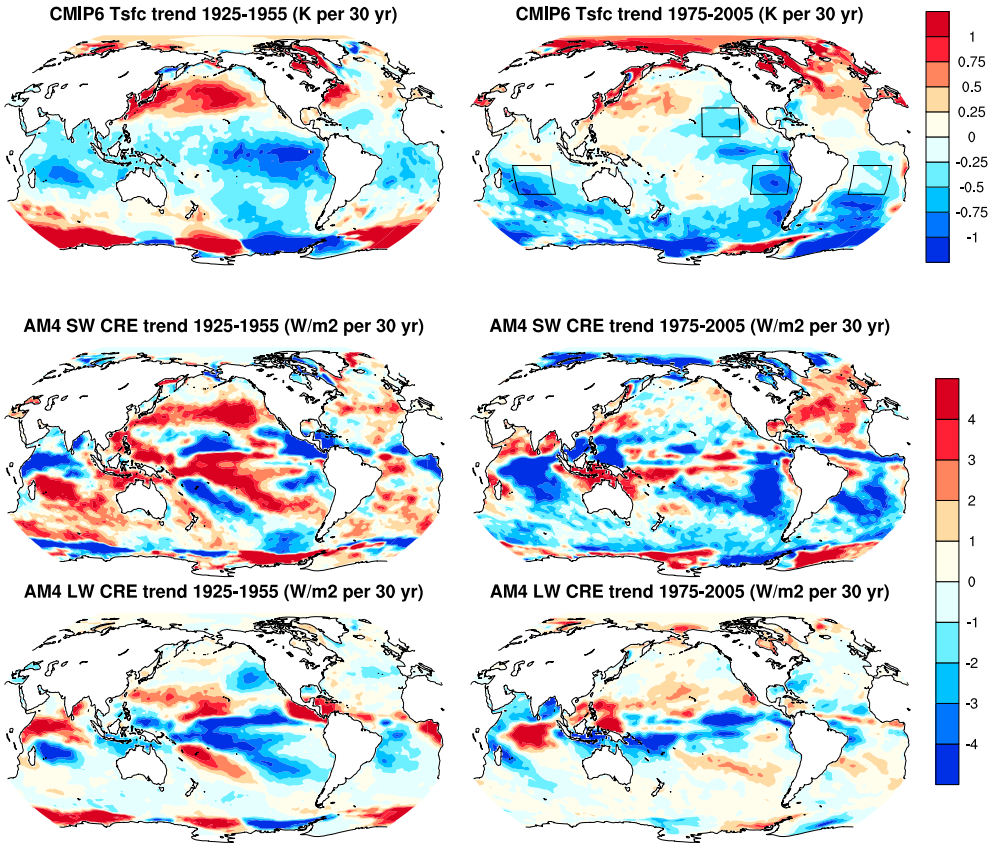

Figure 2. (top row) Trends of observationally derived SST values during periods of high and low sensitivity. To highlight the pattern the mean trend for each period was subtracted. Trends of simulated (AM4.0) (middle row) short-wave (SW) CRE and (bottom row) long-wave (LW) CRE. Left (right) column shows trends between 1925 and 1955 (1975 and 2005). SST fields are from AMIP boundary conditions, PCMDI-AMIP (Taylor et al., 2000). Black boxes in Figure 2 (top right) show window regions discussed in text.

utilizing the moist adiabat (Γ_m^{850}), height on the 700 hPa surface (z_{700}), and the lifting condensation level (LCL). Further details of the boundary conditions, parameterizations, and EIS computation are given in the supporting information.

3. Results

3.1. Contrasting Time Periods of Global Feedback

Strong decadal variability of $-\alpha$ and global low-cloud cover (LCC_{LR}) is shown in Figure 1. The thick lines indicate ensemble mean values for the three different AGCMs; shading indicates the range of ensemble members. Immediately apparent is the period with high sensitivity (small α) centered around approximately 1940. After this the sensitivity of all three models steadily decreases for the remainder of the simulations. This decadal variability is mirrored in the evolution of α_{CRE}, $\alpha_{SW\,CRE}$, and LCC_{LR} (Figures 1c–1e), while the corresponding time series of clear-sky fluxes and $\alpha_{LW\,CRE}$ remain largely constant (Figures 1c and 1f), indicating that the global energy budget is tightly coupled to fluctuations of the total cloud field. The time series of LCC_{LR} in Figure 1d shows that the evolution of global mean LCC anomalies closely tracks with the feedback parameter. This is surprising because we expected radiative effects from high clouds to have a larger influence on α, and while the importance of tropical low-level clouds to the uncertainty of climate sensitivity has been demonstrated (Bony & Dufresne, 2005), the contribution of global mean low-level clouds to the temporal variability of α has been less clear. To quantify the influence of regional changes in LCC on the TOA radiative budget, the LW CRE and SW CRE trends are computed over the two periods of interest (Figure 2). To explore contributions from key geographic regions α is spatially decomposed into windows.

Locations of the windows were chosen to represent regions of importance for stratocumulus clouds between ±30° based on observations (Wood, 2012, his Figure 4a) and our results (Figure 3). The windows used for this

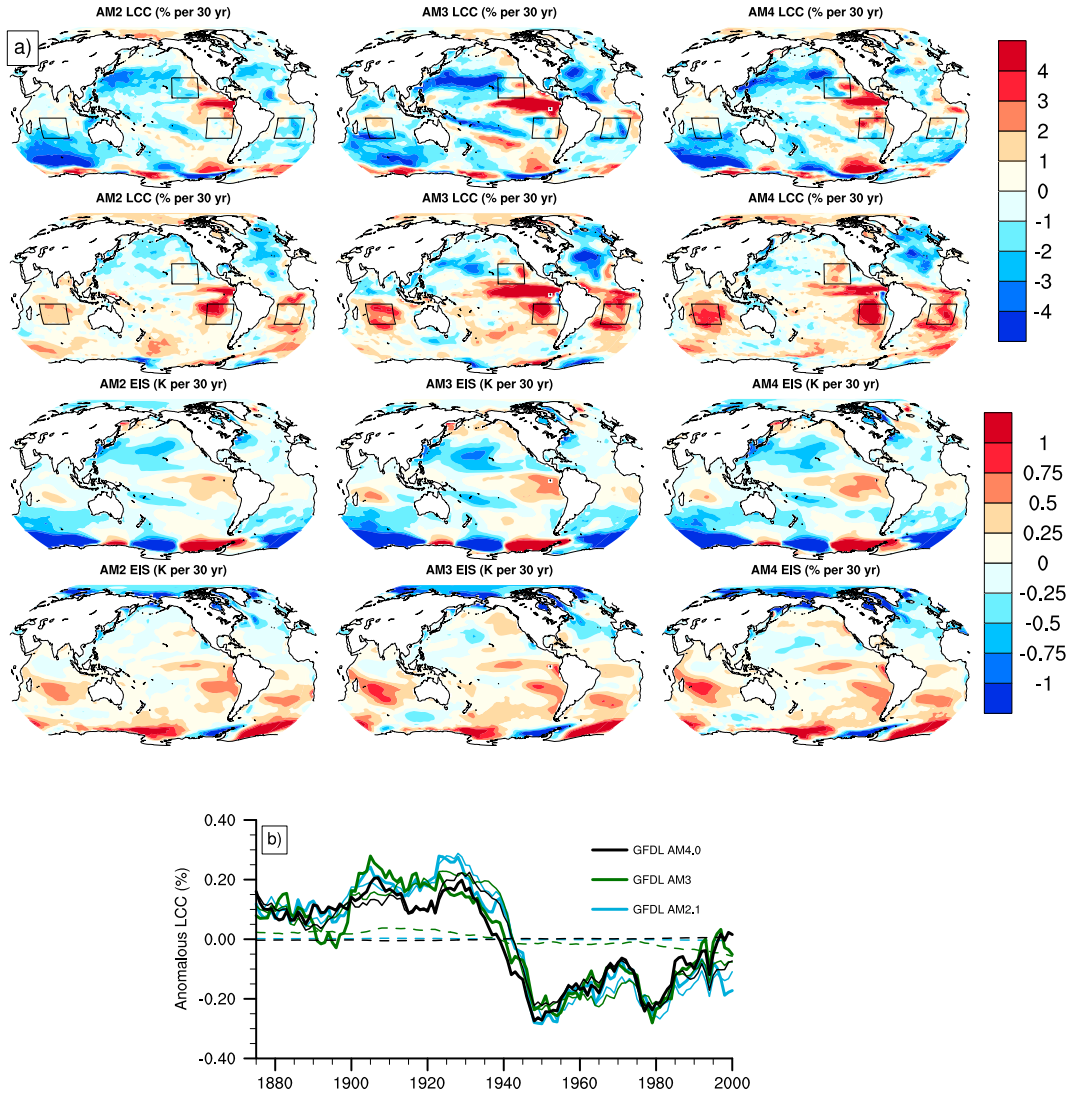

Figure 3. (a) Trends of simulated low-cloud cover (first and second rows) and estimated inversion strength (third and fourth rows). Rows 1 and 3 show trends between 1925 and 1955, rows 2 and 4 show trends between 1975 and 2005. Columns 1–3 show AM2.1, AM3, and AM4.0, respectively. (b) Mean (±60°, 9 year running mean) time evolution of low-cloud cover (ΔLCC) for AM2.1 (blue), AM3 (green), and AM4.0 (black). Thick lines show simulated ΔLCC, and thin lines show ΔLCC approximated using equation (3) with coefficients determined by multiple linear regression (supporting information Table S2). Dashed lines show $\beta\Delta$SST term. Black boxes show window regions discussed in text.

analysis are shown in Figures 2 and 3. The feedback parameter has been computed over particular regions (i) using

$$\overline{T}\alpha_i = \frac{\int N \mathrm{d}A_i}{\int \mathrm{d}A} = N_i w_i \tag{2}$$

with each α_i computed using linear regression of $N_i w_i$ on $\overline{T}$ with a sliding 30 year window and w_i representing the relative area of each window. For the global decomposition used in this study $\sum_i \alpha_i \approx \alpha$ and the variability of α is shown (Figure 1b) to be almost entirely due to the tropics (±30°) minus the windows (compare α from the windows (short dash) with α from the tropics minus the windows (long dash) and with the global mean α). Further, tropical regions typically dominated by stratocumulus do not significantly contribute to the variability of α (Figure 1b; short dashed lines equal sum of α over windows shown in Figures 2 and 3), despite being important for the net radiation budget.

Because there is such a contrast between the "early" period (1925–1955) and the "late" period (1975–2005) in the time series shown in Figure 1, we focus on a comparison between the atmospheric responses to the changing SSTs during these periods. Between 1925 and 1955 the average global feedback parameter for AM4.0, AM3, and AM2.1 changes from values of (−1.6, −1.0, and −1.8 W m^{-2} K^{-1}) to (−2.7, −2.4, and −2.3 W m^{-2} K^{-1}) between 1975 and 1989. This represents a dramatic change in α and determining the cause will be an important part of our ability to understand how clouds respond to SST patterns and thus influence the global energy budget on decadal time scales. Mean LCC, SWCRE, and EIS in each window over both time periods are tabulated in Table S1 in the supporting information. From the early to late period the 30 year trends in the eastern Pacific increased by 2.8% (LCC), decreased by 3.3 W m^{-2} (SWCRE), and increased by 0.2 K (EIS). The other windows show equal or larger changes. Trends in the south Indian window showed LCC increased by 3.8%, SWCRE decreased by 6.7 W m^{-2}, and EIS increased by 0.5 K.

Changing SST patterns are the primary atmospheric driver in these experiments. Anomalous patterns of SST change over each period (trends minus mean trend over that period) are shown in Figure 2. The later period (1975–2005) is characterized by an east-west dipole in the Pacific ocean. As highlighted by Z16, this leads to an increase of LCC in the eastern regions and decreasing cloud feedback. In contrast, the earlier period SST trend is characterized by negative tropical anomalies and positive anomalies in the higher latitudes. We find that the particular response of the low-level clouds to SST patterns differs dramatically between the two periods. In the early period, the midlatitudes are marked by strongly decreasing low-level cloud. In the late period the Southern Hemisphere oceans are almost entirely covered by increasing amounts of low-level cloud (Figure 3). As discussed in the next two sections, there is a clear connection between these SST patterns, the LCC, and EIS fields.

3.2. Dependence of LCC on EIS and SST

The known importance of low-level clouds in the global response to climatic perturbations and the importance of SSTs to the low-level cloud fields motivate us to look at how the LCC evolves during the historical period. We create the anomaly time series, ΔLCC, ΔEIS, and ΔSST by spatially averaging over the region of interest, removing the climatological time mean, and computing yearly mean values for each variable. To probe the dependence of LCC on low-level stability multiple linear regression is used to decompose ΔLCC into a linear combination of ΔEIS and ΔSST. The anomalous changes of tropical marine LCC were shown (Qu et al., 2014; Z16) to be well explained by a linear combination of the change in EIS and SST. The coefficients γ and β can thus be determined for particular experiments or models in the following assumed relationship:

$$\Delta \mathrm{LCC} \approx \gamma \Delta \mathrm{EIS} + \beta \Delta \mathrm{SST}. \tag{3}$$

Between ±30°, $(\gamma, \beta) = (4, 7, -0.13;$ AM2.1), (5.6, −0.53; AM3), and (4.8, −0.39; AM4.0) indicating a model dependent relative contribution from EIS and SST to LCC. Time series of the mean values of anomalous low-cloud cover ΔLCC are shown in Figure 3b (±60°) and supporting information Figure S3 (±30°). Thick lines show the ΔLCC values for each of the three AGCMs, thin lines show the ΔLCC computed with equation 3, and dashed lines show βΔSST. High correlations between ΔLCC and the linear combination of ΔEIS and ΔSST indicate the above relationship is an excellent approximation. Because the three models examined here all use prescribed SSTs, the different values of α and β likely indicates differences in the relative importance of the EIS fields which are in turn driven by the midtropospheric temperature, in this case the temperature at 700 hPa.

Several noteworthy points can be drawn from Figure 3 and supporting information Table S2. Increasing EIS leads to increasing LCC, but increasing SST leads to decreasing LCC. The linear decomposition works well for all three GFDL models, but with differing degrees of dependence among the models on the ΔSST and ΔEIS terms. The relatively flat βΔSST time series in Figure 3 indicate that when the midlatitudes are included, the anomalies of EIS become dominant over the anomalies of SST in determining the changes of LCC. The precipitous drop of anomalous LCC (Figure 3b) corresponds well to the minimum of $\mathrm{LCC}_{\mathrm{LR}}$ and maxima in α_{CRE} and α around 1940 (Figure 1). The successful reconstruction of the mean ΔLCC in the tropics and between ±60 and the close mirroring between the fields of LCC and EIS trends (Figure 3) indicate how closely tied to the SST pattern the LCC and EIS are.

3.3. Response of Clouds to EIS and SST Patterns

The known connections between LCC and SST (Andrews & Webb, 2017; Myers & Norris, 2016; Qu et al., 2014; Zhou et al., 2016) combined with the strong linear dependence of LCC anomalies on the EIS field shown in the previous subsection encourage examination of the global trends of LCC and EIS. A strong relationship

between LCC and EIS in many regions of the globe is seen (Figure 3) with the 30 year trends of LCC and EIS between the late (1975–2005) and early (1925–1955) periods. The response of LCC and EIS to the SST patterns is largely consistent among the three models. Both time periods have an increase of EIS and LCC in the equatorial eastern Pacific Ocean. During the early period the LCC decreases in much of the Southern Hemispheric oceans and northern midlatitudes. During the later period there is an increase of LCC throughout much of the Southern Hemispheric oceans and a decrease of LCC in the north Atlantic and northwest Pacific. This is consistent with a positive CRE (large climate sensitivity) during the early period and a negative CRE (low climate sensitivity) during the later period (Figure 1). Also prominent is the strong Atlantic basin correspondence between LCC and EIS trends during both periods, and the strong shift in the Atlantic from broadly negative trends in the early period to an interhemispheric dipole in the late period. These patterns of LCC modeled during the late period match fairly well with trends of total cloud cover obtained from bias corrected ISCCP observations (supporting information Figure S3).

The trends of LCC (Figure 3, first and second rows) closely mirror the trends of EIS (Figure 3, third and fourth rows) and are related to the SST patterns during both periods. In particular, increasing EIS and LCC occurs in regions of decreasing SST (northeastern and southeastern Pacific, the Indian Ocean, the southern Atlantic, and the Southern Ocean). This relationship has been thoroughly discussed in the literature in the context of stratocumulus regions and subsiding circulations (e.g., Klein & Hartmann, 1993; Myers & Norris, 2013; Qu et al., 2014, 2015; Wood & Bretherton, 2006). Figure 3 shows the relationship to also be important across much of the world ocean. For example, in the early period we see the dominant changes of LCC to be influenced by decreases of EIS over regions with increased SST. There is a clear connection between EIS, SST, and LCC outside of the regions of stratocumulus clouds.

4. Conclusions

We show that low-level clouds in the trade wind regions (±30°) drive the strong decadal variability of the climate feedback parameter over the historical twentieth century. This is distinct from the well-known fact that low-level clouds are also the main source of uncertainty of the ECS among GCMs. Changes in the LCC fields track excellently with α, α_{CRE}, and $\alpha_{SW\,CRE}$ and are consistent with a period of high sensitivity (small α, negative LCC anomalies, and CREs near zero) between 1925 and 1955 and low sensitivity (large α, positive LCC anomalies, and negative CREs) between 1975 and 2005. These changes in the cloud fields are ultimately driven by differences in the SST patterns between the two time periods. The variability is not simply due to a weakening or strengthening of stratocumulus cloud decks, but rather, it is marked by changes in the trade wind regions as a whole and in particular, the tropical Atlantic. The southern ocean low-level clouds also have contrasting trends between the two periods.

We decompose α into specific geographic windows and show the decadal variability of α to be almost entirely due to the tropical region between ±30° (Figure 1b). Large regional changes in the trend of LCC mirror changes in EIS and SWCRE even outside of the regions traditionally thought to be influenced by EIS (Figures 2 and 3). Although specific windows traditionally identified with persistent stratocumulus cloud decks show physically consistent relationships between the LCC, SWCRE, and EIS between the two periods of differing sensitivity, they only contribute a total of around 10% to the magnitude of global mean α (Figure 1b). As computed here, the sum of these windows occupy about 6% of the globe. The same computations with the windows from Qu et al. (2014) accounts for around 13% of α while occupying about 9% of the globe (supporting information Figure S1). In all cases, contributions to the decadal variability of α from particular tropical windows are minimal. Although the small contribution to α from the windows examined here (Figure 1b) is partly due to their small spatial extent relative to the broader tropics, their temporal variability does not match well with that of the global mean α, and it is the absolute contribution to the global mean α which we are interested in.

Following the work of Qu et al. (2014, 2015) and Z16, we use multiple linear regression to estimate the dependence of ΔLCC on ΔEIS and ΔSST for three AGCMs over the historical period. The linear model of LCC change works well when applied to both ±30° and ±60°. The spatial distribution of EIS trends corresponds well to trends of LCC in regions with stratocumulus, trade wind cumulus, and shallow cumulus clouds. This indicates that the strong influence of EIS on LCC holds for disparate patterns of SST and across an α range (in this study) of 2.2 W m^{-2} K^{-1} .

Despite the broad similarity of simulations among the three AGCMs used in this study there are differences. The sensitivities of AM2.1 and AM4.0 are lower than AM3 in the midtwentieth century consistent with a

stronger midlatitude decrease of low-level clouds in AM3 during that period. While ΔLCC of all three AGCMs have a linear dependence on ΔEIS and ΔSST, the relative dependence on each variable differs among models (supporting information Table S2). Over the second half of the twentieth century AM4.0 and AM3 show a strong decrease of α while α_{CRE} decreases by 1.5 W m^{-2} K^{-1} (Figure 1). In contrast, AM2.1 has a weak decrease of α and a decrease of α_{CRE} of only 0.9 W m^{-2} K^{-1} between the two periods.

Recently, Gregory and Andrews (GA16) computed an effective climate sensitivity over the historical period of 2 K. This is significantly less than the sensitivity from the corresponding AOGCMs in response to 4 × CO_2 experiments (Andrews et al., 2012). Similarly, the effective climate sensitivities of AM2.1 (1.7 K), AM3 (2.0 K), and AM4.0 (1.9 K) over the historical period are significantly lower than the ECS of the parent AOGCMs (ESM2M (3.3 K) and CM3(4.8 K), computed from multimillennia equilibrium runs). Much of the uncertainty in the ECS has been attributed to cloud feedbacks (Bony & Dufresne, 2005; Cess et al., 1989). Despite large differences in ECS and effective climate sensitivities among AM2.1, AM3, and AM4.0, this study demonstrates that the cloudy response to changing SST patterns over the historical period is similar for these AGCMs.

Assuming that α is constant has provided a useful approximation of the Earth's energetic response to perturbations despite the knowledge (e.g., Andrews et al., 2012; Andrews et al., 2015; Armour et al., 2013; Senior & Mitchell, 2000) that α is not constant and that the energetic response is nonlinear. Previous work has shown how dependent the equilibrium sensitivity is on low-level clouds in both "fully comprehensive" Earth system models (Paynter & Frölicher, 2015; Sherwood et al., 2014; Vial et al., 2013) as well extremely simplified cases (Silvers et al., 2016). Our analysis of the historical period reveals how dependent temporal variability of α is on changes in the global low-level cloud fields. While the effective climate sensitivity over the historical period is distinct from the ECS, the influence of clouds on the global energy budget is important for both. Because our AGCMs are driven by prescribed SST and sea ice concentrations and constant atmospheric forcing, the relative strength of the feedbacks seen in this study may differ from the feedbacks of a fully interactive Earth system model. But while the cloud feedbacks in the full Earth system may have a more nuanced response, this work clearly documents how the atmospheric cloudy response to particular SST patterns plays a dominant role in the energy budget at the TOA.

Recent work has increasingly highlighted the critical role of cloud base cloudiness in determining the climate sensitivity of GCMs (Brient et al., 2015; Vial et al., 2017). The atmospheric stability (EIS or LTS) provides an excellent diagnostic tool with which to determine how parameterized turbulence and convection influence the low-level atmospheric temperature. This paper shows that EIS simulates LCC very well throughout the global oceans during periods of both high and low sensitivity. Our demonstration of the strong connection between atmospheric stability, LCC, and α indicates a useful link between GCM parameterizations and the climate sensitivity.

Acknowledgments
We thank Mike Winton, Nadir Jeevanjee, and two anonymous reviewers for helpful reviews. Larry Horowitz, Fanrong Zeng, and Tom Delworth are thanked for making data from AM2.1 and AM3 available. Model output is permanently archived at the Geophysical Fluid Dynamics Laboratory; scripts used to analyze data are available from L. G. S. upon request. This paper was prepared by L. G. S. under award NA14OAR4320106 from the National Oceanic and Atmospheric Administration, U.S. Department of Commerce. M.Z. acknowledges partial support by NOAA's Climate Program Office (CPO) Climate Variability and Predictability (CVP) Program (GC14-252) through a CPO CVP funded proposal for understanding AM4/CM4 biases. The statements, conclusions, and recommendations are those of the authors and do not necessarily reflect the views of the National Oceanic and Atmospheric Administration or the U.S. Department of Commerce.

References

Andrews, T. (2014). Using an AGCM to diagnose historical effective radiative forcing and mechanisms of recent decadal climate change. *Journal of Climate*, *27*, 1193–1209.

Andrews, T., Gregory, J. M., Webb, M. J., & Taylor, K. E. (2012). Forcing, feedbacks and climate sensitivity in CMIP5 coupled atmosphere-ocean climate models. *Geophysical Research Letters*, *39*, L09712. https://doi.org/10.1029/2012GL051607

Andrews, T., Gregory, J. M., & Webb, M. J. (2015). The dependence of radiative forcing and feedback on evolving patterns of surface temperature change in climate models. *Journal of Climate*, *28*, 1630–1648.

Andrews, T., & Webb, M. J. (2017). The dependence of global cloud and lapse-rate feedbacks on the spatial structure of tropical Pacific warming. *Journal of Climate*. https://doi.org/10.1175/JCLI-D-17-0087.1

Armour, K. (2017). Energy budget constraints on climate sensitivity in light of inconstant climate feedbacks. *Nature Climate Change*, *7*, 331–335. https://doi.org/10.1038/NCLIMATE3278

Armour, K. C., Bitz, C. M., & Roe, G. H. (2013). Time-varying climate sensitivity from regional feedbacks. *Journal of Climate*, *26*, 4518–4534.

Bony, S., & Dufresne, J. L. (2005). Marine boundary layer clouds at the heart of tropical cloud feedback uncertainties in climate models. *Geophysical Research Letters*, *32*, L20806. https://doi.org/10.1029/2005GL023851

Bony, S., Dufresne, J. L., Treut, H. L., Morcrette, J.-J., & Senior, C. (2004). On dynamic and thermodynamic components of cloud changes. *Climate Dynamics*, *22*, 71–86. https://doi.org/10.1007/s00382-003-0369-6

Bretherton, C. S., Peters, M. E., & Back, L. E. (2004). A new parameterization for shallow cumulus convection and its application to marine subtropical cloud-topped boundary layers. Part I: Description and 1-D results. *Monthly Weather Review*, *132*, 864–882.

Brient, F., Schneider, T., Tan, Z., Bony, S., Qu, X., & Hall, A. (2015). Shallowness of tropical low clouds as a predictor of climate models' response to warming. *Climate Dynamics*, *45*. https://doi.org/10.1007/s00382-015-2846-0

Cess, R. D., Potter, G. L., & Blanchet, J. (1989). Interpretation of cloud-climate feedback as produced by 14 atmospheric general circulation models. *Science*, *245*, 513–516.

Donner, L. J. (1993). A cumulus parameterization including mass fluxes, vertical momentum dynamics, and mesoscale effects. *Journal of Atmospheric Sciences*, *50*, 889–906. https://doi.org/0.1175/1520-0469(1993)050<0889:ACPIMF>2.0.CO;2

Donner, L. J., Wyman, B. L., Hemler, R. S., Horowitz, L. W., Ming, Y., Zhao, M., … Zeng, F. (2011). The dynamical core, physical parameterizations, and basic simulation characteristics of the atmospheric component AM3 of the GFDL global coupled model CM3. *Journal of Climate*, *24*, 3484–3519. https://doi.org/10.1175/2011JCLI3955.1

Forster, P. M., & Gregory, J. M. (2006). The climate sensitivity and its components diagnosed from Earth radiation budget data. *Journal of Climate*, *19*, 39–52. https://doi.org/10.1175/JCLI3611.1

Flato, G., Marotzke, J., Abiodun, B., Braconnot, P., Chou, S. C., Collins, W., … Rummukainen, M. (2013). Evaluation of climate models, *Climate change 2013: The physical science basis. Contribution of Working Group I to the Fifth Assessment Report of the Intergovernmental Panal on Climate Change* (pp. 741–882). Cambridge: Cambridge University Press. https://doi.org/10.1017/cbo9781107415324.020

GFDL-GAMDT (2004). The new GFDL global atmosphere and land model AM2/LM2: Evaluation with prescribed SST simulations. *Journal of Climate*, *17*, 4641–4673. https://doi.org/10.1175/JCLI-3223.1

Gregory, J. M., & Andrews, T. (2016). Variation in climate sensitivity and feedback parameters during the historical period. *Geophysical Research Letters*, *43*, 3911–3920. https://doi.org/10.1002/2016GL068406

Gregory, J. M., Ingram, W. J., Palmer, M. A., Jones, G. S., Stott, P. A., Thorpe, R. B., … Williams, K. (2004). A new method for diagnosing radiative forcing and climate sensitivity. *Geophysical Research Letters*, *31*, L03205. https://doi.org/10.1029/2003GL018747

Grise, K. M., & Medeiros, B. (2016). Understanding the varied influence of midlatitude jet position on clouds and cloud radiative effects in observations and global climate models. *Journal of Climate*, *29*, 9005–9025. https://doi.org/10.1175/JCLI-D-16-0295.1

Haugstad, A. D., Armour, K. C., Battisti, D. S., & Rose, B. E. J. (2017). Relative roles of surface temperature and climate forcing patterns in the inconstancy of radiative feedbacks. *Geophysical Research Letters*, *44*, 7455–7463. https://doi.org/10.1002/2017GL074372

Klein, S. A., & Hartmann, D. L. (1993). The seasonal cycle of low stratiform clouds. *Journal of Climate*, *6*, 1587–1606. https://doi.org/10.1175/1520-0442(1993)006<1587:TSCOLS>2.0.CO;2

Mauritsen, T., Graversen, R. G., Klocke, D., Langen, P. L., Stevens, B., & Tomassini, L. (2013). Climate feedback efficiency and synergy. *Climate Dynamics*, *41*, 2539–2554.

Medeiros, B., Stevens, B., Held, I. M., Zhao, M., Williamson, D. L., Olson, J. G., & Bretherton, C. S. (2008). Aquaplanets, climate sensitivity, and low clouds. *Journal of Climate*, *21*, 4974–4991.

Moorthi, S., & Suarez, M. (1992). Relaxed Arakawa Schubert: A parameterization of moist convection for general circulation models. *Monthly Weather Review*, *120*, 978–1002.

Myers, T. A., & Norris, J. R. (2013). Observational evidence that enhanced subsidence reduces subtropical marine boundary layer cloudiness. *Journal of Climate*, *26*, 7507–7524. https://doi.org/10.1175/JCLI-D-12-00736.1

Myers, T. A., & Norris, J. R. (2016). Reducing the uncertainty in subtropical cloud feedback. *Geophysical Research Letters*, *43*, 2144–2148. https://doi.org/10.1002/2015GL067416

Paynter, D., & Frölicher, T. (2015). Sensitivity of radiative forcing, ocean heat uptake, and climate feedback to changes in anthropogenic greenhouse gases and aerosols. *Journal of Geophysical Research: Atmospheres*, *120*, 9837–9854. https://doi.org/10.1002/2015JD023364

Popp, M., & Silvers, L. G. (2017). Double and single ITCZs with and without clouds. *Journal of Climate*, *30*, 9147–9166. https://doi.org/10.1175/JCLI-D-17-0062.1

Proistosescu, C., & Huybers, P. J. (2017). Slow climate mode reconciles historical and model-based estimates of climate sensitivity. *Science of Advanced*, *3*, E1602821. https://doi.org/10.1126/sciadv.1602821

Qu, X., Hall, A., Klein, S. A., & Caldwell, P. M. (2014). On the spread of changes in marine low cloud cover in climate model simulations of the 21st century. *Climate Dynamics*, *42*, 2603–2626. https://doi.org/10.1007/s00382-013-1945-z

Qu, X., Hall, A., Klein, S. A., & Caldwell, P. M. (2015). The strength of the tropical inversion and its response to climate change in 18 CMIP5 models. *Climate Dynamics*, *45*, 375–396. https://doi.org/10.1007/s00382-014-2441-9

Randall, D. A., Coakley, J. J. A., Fairall, C., Kropfli, R. A., & Lenschow, D. H. (1984). Outlook for research on subtropical marine stratiform clouds. *Bulletin of the American Meteorological Society*, *65*, 1290–1301.

Rose, B. E., Armour, K. C., Battisti, D. S., Feldl, N., & Koll, D. D. B. (2014). The dependence of transient climate sensitivity and radiative feedbacks on the spatial pattern of ocean heat uptake. *Geophysical Research Letters*, *41*, 1071–1078. https://doi.org/10.1002/2013GL058955

Rose, B. E., & Rayborn, J. (2016). The effects of ocean heat uptake on transient climate sensitivity. *Current Climate Change Reports*, *2*, 190–201. https://doi.org/10.1007/s40641-016-0048-4

Senior, C. A., & Mitchell, J. F. B. (2000). The time-dependence of climate sensitivity. *Geophysical Research Letters*, *27*, 2685–2688. https://doi.org/10.1029/2012GL051607

Sherwood, S. C., Bony, S., & Dufresne, J. L. (2014). Spread in model climate sensitivity traced to atmospheric convective mixing. *Nature*, *505*, 37–42. https://doi.org/10.1038/nature12829

Silvers, L. G., Stevens, B., Mauritsen, T., & Giorgetta, M. (2016). Radiative convective equilibrium as a framework for studying the interaction between convection and its large-scale environment. *Journal of Advances in Modeling Earth Systems*, *8*, 1330–1344. https://doi.org/10.1002/2016MS000629

Taylor, K. E., Williamson, D., & Zwiers, F. (2000). The sea surface temperature and sea-ice concentration boundary conditions of AMIP II simulations (PCMDI Report 60). California: Lawrence Livermore National Laboratory Program for Climate Model Diagnosis and Intercomparison. https://doi.org/10.1175/JCLI-D-17-0062.1

Vial, J., Dufresne, J.-L., & Bony, S. (2013). On the interpretation of inter-model spread in CMIP5 climate sensitivity estimates. *Climate Dynamics*, *41*, 3339–3362. https://doi.org/10.1007/s00382-013-1725-9

Vial, J., Bony, S., Stevens, B., & Vogel, R. (2017). Mechanisms and model diversity of trade-wind shallow cumulus cloud feedbacks: A review. *Surveys in Geophysics*, *38*, 1331–1353. https://doi.org/10.1007/s10712-017-9418-2

Webb, M. J., Lock, A. P., Bretherton, C. S., Bony, S., Cole, J. N., Idelkadi, A., … Zhao, M. (2015). The impact of parameterized convection on cloud feedback. *Philosophical Transactions of the Royal Society of London, Series A: Mathematical, Physical and Engineering Sciences*, *373*, 20140414. https://doi.org/10.1098/rsta.2014.0414

Webb, M. J., Andrews, T., Bodas-Salcedo, A., Bony, S., Bretherton, C. S., Chadwick, R., … Watanabe, M. (2017). The cloud feedback model intercomparison project (CFMIP) contribution to CMIP6. *Geoscientific Model Development*, *10*, 359–384. https://doi.org/10.5194/gmd-10-359-2017

Winton, M., Takahashi, K., & Held, I. M. (2010). Importance of ocean heat uptake efficacy to transient climate change. *Journal of Climate*, *23*, 2333–2344. https://doi.org/10.1175/2009JCLI3139.1

Wood, R. (2012). REVIEW stratocumulus clouds. *Monthly Weather Review*, *140*, 2373–2423. https://doi.org/10.1175/MWR-D-11-00121.1

Wood, R., & Bretherton, C. S. (2006). On the relationship between stratiform low cloud cover and lower-tropospheric stability. *Journal of Climate*, *19*, 6425–6432. https://doi.org/10.1175/JCLI3988.1

Zhao, M., Golaz, J.-C., Held, I. M., Ramaswamy, V., Lin, S.-J., Ming, Y., … Paynter, D. (2016). Uncertainty in model climate sensitivity traced to representations of cumulus precipitation microphysics. *Journal of Climate*, *29*, 543–560. https://doi.org/10.1175/JCLI-D-15-0191.1

Zhou, C., Zelinka, M. D., & Klein, S. A. (2016). Impact of decadal cloud variations on the Earth's energy budget. *Nature Geoscience*, *9*, 871–874. https://doi.org/10.1038/ngeo2828